Contrib Mineral Petrol (2006) 151: 665–680
DOI 10.1007/s00410-006-0086-3

ORIGINAL PAPER

Cliff S. J. Shaw

Effects of melt viscosity and silica activity on the rate and mechanism of quartz dissolution in melts of the CMAS and CAS systems

Received: 5 October 2005 / Accepted: 9 March 2006 / Published online: 19 April 2006

Abstract The dissolution rate of quartz in melts of the CMAS and CAS systems at 1,600°C and 1.5 GPa is a function of both the silica activity of the melt and its viscosity. In melts with low silica activity quartz dissolves more quickly than in higher $aSiO_2$ melts regardless of viscosity. For melts with equal $aSiO_2$, dissolution is faster in the low viscosity melt. Quartz dissolution is controlled by interface kinetics in three of the four melts used in this study for times much greater than predicted by the model of Zhang et al. (in Contrib Mineral Petrol 102:492–513 1989). One melt which was previously shown to adhere to the predicted behaviour at lower temperature shows a significant activation time at higher temperature. All the dissolution data indicate that there are likely to be three distinct domains of dissolution behaviour, although the details of why a particular melt falls in any one domain require further study. Although the current database is small, the relationship between quartz solubility and the dissolution constant indicate that solubility may be a useful parameter for predicting dissolution rates, particularly if silica activity and melt viscosity are also known.

Introduction

The nature and rate of reactions between silicate melts and crystalline material are of fundamental importance to our understanding of the petrogenesis and ascent of magma, the synthesis of glass and smelting processes involving oxide melts (Apanina 1984; Avramov et al. 1979; Barnes et al. 2004; Brearley and Scarfe 1986; Kalyanram and Bell 1960; Maury and Didier 1991).

The rate at which minerals dissolve in silicate melts affects the efficiency of assimilation, thus dissolution rates can affect the major and trace element as well as the isotopic composition of magmas during their passage through the mantle and crust. Efficient assimilation of mantle minerals can lead to significant changes in the composition of the melts and the mantle (Kelemen et al. 1992; Shaw et al. 2005). Similarly, minerals in crustal and mantle xenoliths that dissolve slowly may survive as xenocrysts (Shaw 2004b; Watson 1996), whereas those that dissolve quickly will be completely assimilated and their presence may only be detected through the trace element or isotopic signature of the solidified magma (Gurenko et al. 2001). In addition, the effects of uphill diffusion and multicomponent mixing may lead to complex chemical trends that cannot be modelled by simple linear mixing (Chakraborty et al. 1995; Shaw 1999; Zhang et al. 1989).

The mechanism of dissolution is also important in magmatic systems, since the overall rate will be controlled by the slowest of several simultaneous reactions. On the basis of an analysis of the reaction– diffusion equation and their experiments on mineral dissolution rates Zhang et al. (1989) suggested that in most magmas, the rate-controlling step in dissolution should be diffusion in the melt and the critical time required for diffusion to become rate-controlling should be less than 1 s. This, together with the work of Liang (1999), implies that in a non-convecting system, the dissolution rate of a mineral in a magma can be predicted if the various elements of the diffusion matrix are known or can be measured. However, experiments by Acosta-Vigil et al. (2002, 2006), Hammouda and Pichavant (1999) and Shaw (2004a) indicate that for some mineral–melt pairs there is an activation time three to five orders of magnitude greater than that suggested by Zhang et al. (1989) during which interface reaction, rather than diffusion in the melt, is the rate-controlling step. Although these activation times are only of the order of minutes to

Communicated by J. Hoefs

C. S. J. Shaw
Department of Geology, University of New Brunswick,
2 Bailey Drive, Fredericton, NB, Canada E3B 5A3
E-mail: cshaw@unb.ca
Tel.: +1-506-4473195
Fax: +1-506-4535055

hundreds of hours, they may be significant in the dynamic world of the magma chamber.

Kerr (1995) developed equations that relate dissolution rates to diffusion during free convection on the assumption that both the dissolution mechanism and rate are fixed. If, for some mineral–melt pairs, the dissolution mechanism is time dependent, as suggested by Shaw (2004a), there will be a periodic switch in the dissolution mechanism. During the activation period, dissolution will be controlled by interface kinetics and reaction will be slower than predicted from the diffusion model. Once the critical time is reached, diffusion becomes rate controlling and it is possible to make predictions of dissolution rate from this point. However, at some time after the onset of diffusion control, the boundary layer may become unstable and rise off the interface to be replaced by fresh melt (cf. Shaw 2000). At this point dissolution is again controlled by interface kinetics. This cycle may continue until the mineral is completely dissolved or the bulk melt composition changed. The rate of dissolution will also change as the mechanism changes; however, whether there will be an increase or decrease in the rate will depend on the composition of the mineral–melt couple.

Many previous studies of mineral–melt reactions have examined the effects of external controls such as temperature, crystal rotation rate, or pressure, on the rate and mechanism of mineral dissolution (Acosta-Vigil et al. 2002; Brearley and Scarfe 1986; Canil and Fedortchouk 1999; Cooper and Kingery 1964; Donaldson 1985; Shaw 1999, 2000, 2004a; Shaw et al. 1998; Zhang et al. 1989), but few have dealt with the fundamental factors that control the dissolution process, i.e. the activity of components, the solubility of the crystalline phase and the diffusivity of the released cations in the melt. Edwards and Russell (1996, 1998) examined the dissolution process in terms of the thermodynamic affinity of the dissolving mineral; however, this relied on data from earlier experimental studies, some of which were difficult to interpret because of complexities introduced by compositional convection (see Shaw 2000).

Donaldson (1990) and Shaw (2004a) have suggested that there is a link between dissolution mechanism, magma composition and magma viscosity; however, they were unable to separate the effects of composition from those of viscosity. The purpose of this study therefore is to investigate the effects of $aSiO_2$ and melt viscosity on quartz dissolution rates and mechanisms in CAS and CMAS melts at 1,600°C and 1.5 GPa.

Starting materials and experimental and analytical methods

To examine the effects of viscosity on quartz dissolution rates, independent of silica activity, four melt compositions were prepared (Table 1). Two of these have silica activity of 0.47 and one atmosphere viscosities of 3.44 and 1.08 Pa s, respectively, at 1,600°C. The other two have silica activity of 0.26 and one atmosphere viscosities of 1.17 and 0.34 Pa s at 1,600°C. In order to achieve the similarity in $aSiO_2$ with a reasonable variation in viscosity, the melts chosen were in the CMAS and CAS systems. The difference in viscosity between the melts is small; however, the predictions of Shaw (2004a) suggest that there should be measurable differences in the dissolution rate.

The solvents used were melts CMAS 6 and CMAS 3 of Shaw (2004a). The higher viscosity CAS melts were CAS 1 which has the same silica activity as CMAS 6 and is the solvent melt used by (Liang 1999). Melt CAS 2 was constrained to have the same silica activity as CMAS 3 by iteratively calculating the thermodynamic properties of various compositions using the MELTS supplementary calculator (Ghiorso and Sack 1995). For the compositions chosen, homogeneous glasses were produced by fusion of Analar grade oxides at 1,650°C in Pt crucibles. Each composition was fused three times and lightly crushed between fusions. After the final fusion, the glass was ground to a fine powder in an agate mortar. Nominal and analysed compositions of the glasses are given in Table 1.

The viscosity of the four melts used in this study as well as the melts used in the earlier study of Shaw (2004a) were measured directly. In previous studies, the viscosity of the solvent melts was calculated; however, in many cases there are large differences between the real and calculated viscosities of silicate melts (see Table 1). Since the viscosity is thought to be such an important parameter in dissolution, direct measurement is preferable.

Viscosities were determined using the concentric cylinder method. A Brookfield DV-III (RV) viscometer with a $Pt_{80}Rh_{20}$ spindle and a $MoSi_2$ box furnace were used to measure melt viscosities in a $Pt_{80}Rh_{20}$ crucible. Further details of the methods used can be found in Dingwell (1989). For each experiment, the initial rotation rate was 40 rpm and the initial temperature was 1,625°C. This initial temperature was held for 2 h with subsequent steps having a 1 h dwell. Temperature was reduced at 200°C per minute in 10–25°C steps until crystallization occurred. The viscosity of the samples was calculated using a calibration of the crucible, spindle and viscometer with glass standard DGG-1 (see Toplis and Dingwell (2004) for discussion of the precision and accuracy of the equipment).

Quartz discs were cut, using a diamond wire saw, from rods cored parallel to the *C*-axis of a large single crystal from Brazil. The discs were polished to a 1-μm finish before measuring with a micrometer. Disks that showed initial variations in thickness around their circumference of more than 10 μm were discarded. The thickness measurements are accurate to within ±2 μm based on comparison with a standard.

Table 1 Starting compositions for experiments

	CAS 1			CMAS 6			CAS 2			CMAS 3		
wt %	Nominal	Analysed	SD	Nominal	Analysed	SD	Nominal	Analysed	SD	Nominal	Analysed	SD
SiO_2	59.35	59.71	(0.37)	54.44	54.90	(0.65)	50.00	50.21	(0.71)	44.35	44.69	(0.27)
Al_2O_3	15.31	14.70	(0.04)	15.58	15.01	(0.07)	17.50	16.97	(0.09)	17.96	17.32	(0.03)
MgO				15.47	15.34	(0.27)				24.96	24.81	(0.06)
CaO	25.34	25.55	(0.09)	14.51	14.73	(0.03)	32.50	32.73	(0.01)	12.73	13.08	(0.06)
Total	100.00	99.96		100.00	99.98		100.00	99.91		100.00	99.90	
Mole fraction												
SiO_2	0.47096			0.43009			0.25167			0.220360		
Al_2O_3	0.13195			0.14431			0.17098			0.192623		
Mg_2SiO_4				0.18125						0.338727		
$CaSiO_3$	0.39709			0.24436			0.57734			0.248290		
Silica activity[a]	1,600°C, 1.5 GPa											
	0.475			0.468			0.257			0.258		
Measured viscosity (Pa s) 1,600°C (1 atm)												
	3.44			1.08			1.17			0.34		
Calculated viscosity (Pa s) 1,600°C[b]												
	20.50			1.26			2.66			0.14		
NBO/T[c]	0.47			0.81			0.69			1.23		

Properties were calculated for the nominal compositions
[a]Calculated using MELTS (Ghiorso and Sack 1995)
[b]Calculated using Shaw (1972)
[c]Calculated using Mysen et al. (1984)

All experiments were performed at 1,600°C and 1.5 GPa in 1/2-in. talc–Pyrex pressure cells in the 150-tonne end-loaded piston cylinder press at the University of New Brunswick. Isothermal conditions were chosen since this temperature is significantly above the liquidus temperature of the melts and fills a gap in the temperature range of previous experiments that allows a better determination of the activation energy of dissolution for several of the solvent melts. The experiments were designed to eliminate convection in the melt by placing the quartz disc on the top of the melt column and also by minimizing the temperature gradient in the capsule.

Three different encapsulation techniques were used. Early experiments were performed using the same method outlined in Shaw (2004a); however, it proved extremely difficult to keep the CAS glasses completely dry during the set up of the experiments, and all the initial experiments showed distinct heterogeneity in the glass composition because of hydrogen diffusion. The second series of experiments followed the same method as outlined by Liang (1999); these too proved problematic because the small difference in the diameter of the Pt-encased glass sleeve and the quartz disc led to the development of an extremely irregular quartz–melt interface, particularly in experiments with very low viscosity melts. Tests of Mo solubility under the desired conditions with all four solvents showed that Mo contents were below the detection limits of the electron microprobe after durations of 10 h. Thus all of the data reported here are from experiments performed in Mo capsules with no Pt sleeve. The Mo capsules were surrounded by a boron nitride sleeve and placed in tapered graphite furnaces (to minimize the thermal gradient) in a talc–Pyrex pressure cell (see Shaw 2004a). The experiments were heated to 1,600°C at 300°C per minute with a 6-min dwell at 1,000°C. Temperature was controlled using a type C thermocouple together with a Eurotherm 818 temperature controller. Temperature was not corrected for the effects of pressure on the thermocouple EMF and a friction correction of 18% was applied to nominal pressures based on calibrations using the melting point of gold, NaCl and diopside.

Experiments were run for 0.5–720 min and then quenched by turning off the power to the furnace while keeping pressure within 5% of the run value. All samples cooled from the run temperature to 800°C within 6–7 s at $\sim$ 110°C s^{-1}. Although the cooling rate decreased at temperatures below 800°C, all samples reached room temperature within 40 s of quenching. Samples were set in epoxy under vacuum and ground to expose the middle of the capsule then polished to a 1-μm finish.

In addition to the dissolution experiments, several equilibration experiments were performed to locate the quartz liquidus surface in the CMAS and CAS systems at 1,600°C and 1.5 GPa.

The charges were examined in reflected light and with a Jeol 6400 SEM to chracterise the texture of the interface. Compositional data were obtained along traverses perpendicular to the interface using a Jeol 733 electron microprobe with Geller Microanalytical automation. All samples were analysed at 15 kV and 10 nA with count times of 20 s on peaks and 10 s on each background. Standards were plagioclase for Si, Al and Ca and olivine for Mg. All data were reduced using the ZAF correction routine.

Data processing

The amount of quartz dissolved during the CAS–CMAS experiments can be determined in two ways. First by direct measurement of the disc thickness before and after each run. In cases where dissolution is fairly rapid this method gives acceptable results; however, in cases where the dissolution rate is low, small variations in the initial size of the crystal can lead to significant uncertainties in the determinations of the amount of quartz dissolved. For this reason, dissolution amounts were determined by mass balance using the following formulation (Zhang et al. 1989):

$$\int_0^{\infty} \left(\frac{\rho}{\rho_{\infty}} C - C_{\infty}\right) \mathrm{d}x = \frac{\rho_s}{\rho_{\infty}} L_s C_s - L C_{\infty}, \quad (1)$$

where C is concentration at any point x, where x is the distance to the mineral–melt interface, C_{∞} is the far field melt composition, C_s is the concentration in the crystal, ρ is the density of the melt at any point x, ρ_{∞} is the density of the far field melt, ρ_s is the density of the crystal, L_s is the crystal dissolution distance and L is the melt growth distance. These calculations were performed on closely spaced electron microprobe traverses taken normal to the quartz–melt interface. The value of the integral on the left-hand side of the equation was determined from a least squares fit of the electron microprobe data to an error function type diffusion equation. On the right-hand side of Eq. 1 the values of C_s and C_{∞} are known, the crystal and melt densities were calculated using the partial molar volume data of Lange and Carmichael (1987). The amount of dissolution (L_s) is related to the melt growth distance by

$$L = L_s \frac{\rho_s}{\rho_{\infty}}. \quad (2)$$

In all cases the r^2 of the fit was between 0.980 and 0.996. The amount of dissolution calculated by this method is presented in Table 2.

Results

Viscosity

Since the measured viscosity and that calculated using the model of Shaw (1972) do not match particularly well (Table 1), the solvent melts used in the study of Shaw (2004a) were also measured to allow a more complete discussion of the effects of viscosity. The results from these measurements are also presented in Table 3 and in Fig. 1. Composition CMAS 1 was not measured during this study as it was partially crystallized at the maximum attainable temperature. All the data were fit by an Arrhenius relation of the form:

$$\eta = \eta_o \exp\left(\frac{E}{RT}\right) \quad (3)$$

Where E is the activation energy, R is the gas constant and T the absolute temperature. From this relation the viscosity can be calculated beyond the measurement range, assuming Arrhenian behaviour, and the activation energy for viscous flow can be calculated (Table 3). Use of an Arrhenian model for viscosity means that extrapolations to lower temperature must be made with care, bearing in mind that some of these melts will be fragile and will therefore show non-Arrhenian behaviour.

CAS 1 is the most viscous of the solvent melts used in this study. CMAS 3 is approximately an order of magnitude less viscous. Melts CAS 2 and CMAS 6 have intermediate and very similar viscosity (Fig. 1). The

Table 2 Experiment durations and dissolution amounts calculated using Eq. 1

Sample	Duration (s)	Solvent	Amount dissolved[a] (μm)
Dissolution experiments			
Mo13	1,000	CAS 1	17
Mo10	2,730	CAS 1	56
Mo8	3,600	CAS 1	71
Mo50	3,600	CAS 1	90
Mo24	5,000	CAS 1	87
Mo14	10,000	CAS 1	170
Mo25	10,000	CAS 1	129
Mo15	20,000	CAS 1	256
Mo 11	25,500	CAS 1	236
Mo18	300	CAS 2	43
Mo21	600	CAS 2	90
Mo17	900	CAS 2	83
Mo19	1,500	CAS 2	118
Mo22	1,800	CAS 2	93
Mo27	1,800	CAS 2	102
Mo23	2,700	CAS 2	144
Mo20	3,600	CAS 2	173
Mo51	3,630	CAS 2	144
Mo28	6,000	CAS 2	229
Mo16	7,200	CAS 2	247
Mo36	30	CMAS 6	26
Mo35	300	CMAS 6	54
Mo34	600	CMAS 6	64
Mo49	900	CMAS 6	77
Mo32	1,800	CMAS 6	94
Mo31	2,400	CMAS 6	115
Mo37	3,600	CMAS 6	152
Mo44	300	CMAS 3	127
Mo52	600	CMAS 3	150
Mo43	900	CMAS 3	156
Mo42	1,800	CMAS 3	239
Mo45	3,000	CMAS 3	249
Mo39	3,600	CMAS 3	274
Equilibration experiments			
Mo 53	21,600	All melts	
Mo54	43,200	All melts	

[a]Calculated by mass balance (see Eq. 1)

Table 3 Viscosity determinations in Pa s

Temperature (°C)	*CAS 1*	*CAS 2*	CMAS 2	*CMAS 3*	CMAS 4	CMAS 5	*CMAS 6*	CMAS 7
1,300	*87.127*							
1,325	*59.866*							
1,350	*42.582*	*10.932*						
1,375	*30.915*	*8.152*					*7.664*	15.027
1,400	*22.951*	*6.213*				2.954	*5.871*	11.766
1,425	*17.051*	*4.777*				2.326		8.954
1,450	*12.837*	*3.770*				1.876	*3.585*	6.913
1,475	*10.475*	*3.027*		*0.744*	0.448	1.511		5.415
1,500	*8.191*	*2.446*		*0.620*	0.382	1.231	*2.296*	4.309
1,525	*6.516*	*2.003*		*0.528*	0.332	1.012		3.456
1,535				*0.497*				
1,545				*0.467*				
1,550	*5.212*	*1.654*			0.284	0.840	*1.541*	2.799
1,555			0.399	*0.437*				
1,565			0.389	*0.404*				
1,575	*4.205*	*1.391*	0.373	*0.382*	0.247	0.700		2.286
1,585			0.352	*0.365*				
1,595			0.341	*0.350*				
1,600	*3.442*	*1.172*			0.219	0.588	*1.082*	1.874
1,605			0.331	*0.327*				
1,615			0.316	*0.312*	0.204			
1,625	*2.832*	*0.989*	0.309	*0.291*	0.196	0.495	*0.905*	1.555
1,650	*2.345*							
Activation energy (kJ/mol)	256.6 ± 0.1	253.6 ± 0.1	110.6 ± 0.2[a]	170.3 ± 0.5	153.2 ± 0.3	208.9 ± 0.04	221.7 ± 0.1	237.4 ± 0.1
Pre-exponential (Pa s)	$2.34 \times 10^7 \pm 2.50 \times 10^8$	$7.20 \times 10^8 \pm 1.68 \times 10^9$	$2.77 \times 10^4 \pm 1.63 \times 10^6$	$5.97 \times 10^6 \pm 1.58 \times 10^7$	$1.18 \times 10^5 \pm 1.10 \times 10^7$	$8.72 \times 10^7 \pm 3.25 \times 10^9$	$6.98 \times 10^7 \pm 1.60 \times 10^8$	$4.46 \times 10^7 \pm 4.05 \times 10^9$

Samples in italics are those used in this study. All other samples are from Shaw (2004a)
[a]Data limited to a 70°C temperature range

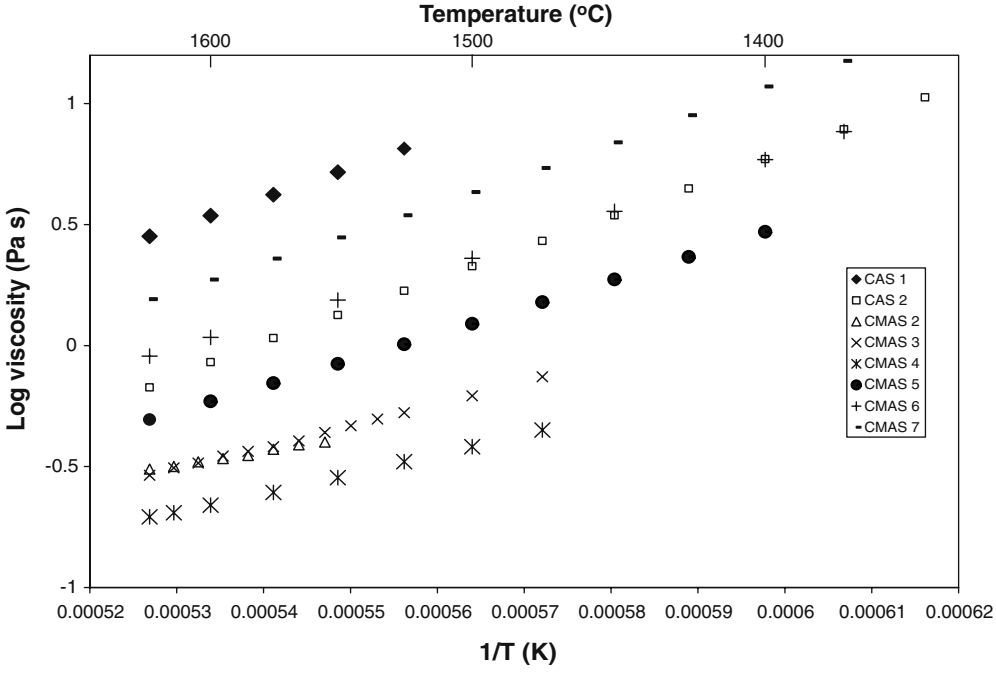

Fig. 1 Arrhenius plot of the viscosity data for the melts used in this study and the melts used in Shaw (2004a)

calculated activation energy for flow is greatest for the melts in the CAS system and lower in the CMAS melts, even for melts of approximately the same viscosity at the experimental temperature (Table 3).

Texture

As in the earlier experiments of Shaw (2004a), experiments with the low viscosity CMAS 3 solvent commonly

have small, 5–10 micron, pendant quartz quench crystals at the interface with the partly dissolved quartz disc. In addition, several samples with this solvent contain abundant quench crystals of olivine that are preferentially located in the far field region of the capsule, i.e. farthest away from the quartz disc. In all cases, the interface between the quartz disc and the solvent melt is sharp and planar (Fig. 2). Both the disc and the solvent melt are cut by numerous fractures that are a result of unloading during decompression. Analysis of concentration profiles across cracks is difficult because it is impossible to directly determine the displacement, if any, across the cracks. In order to avoid uncertainties in the distance from the interface, several profiles were analysed where cracks were intersected at different distances from the interface (Fig. 2). All of these profiles were combined so that the displacement across cracks could be defined and its effects removed (see also Zhang et al. 1989).

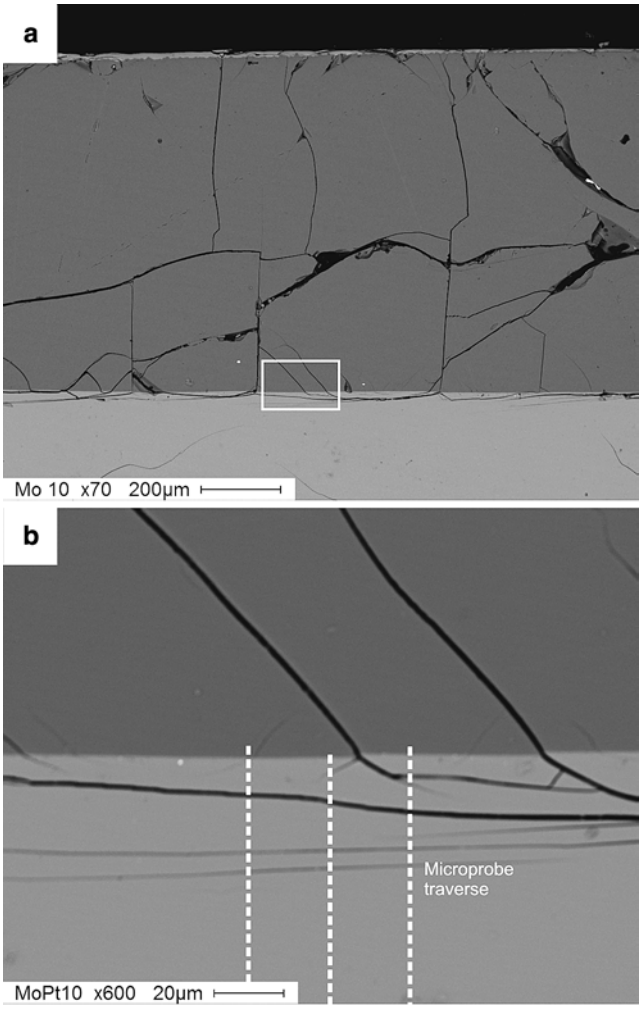

Fig. 2 Backscattered electron images of a typical quartz melt interface (Mo10–melt CAS1 2,730 s) showing the sharp planar interface between the quartz disc and the solvent melt and the position of electron microprobe traverses

Dissolution rates

All previous studies of dissolution in convection-free melts have determined that the dissolution amount is a function of the square root of time. This has been interpreted to be a result of diffusion control of the dissolution reaction. In common with previous studies all of the dissolution data (Table 2) are best fit by an equation of the form:

$$u = a + bt^{0.5} \tag{4}$$

the r^2 value for all the fits shown in Fig. 3 is 0.94 or better (Table 4). The negative intercept for both CAS melts indicates either a brief time lag before dissolution began or is a result of error in the measurement and fitting process. The positive intercept for both CMAS melts suggests that there was some dissolution of quartz during the heating stage of the experiments.

Within each compositional group (CMAS or CAS) the dissolution rate increases as the silica activity decreases (Fig. 3a), in agreement with the results of Shaw (2004a). For the melts with the same silica activity, dissolution is faster in the lower viscosity melt (Fig. 3a).

Figure 3b, c show the data from this study compared to dissolution rates obtained for the same compositions by Liang (1999); and Shaw (2004a); for clarity only the fitted curves from these previous studies are shown. These plots show that the dissolution rates obtained in this study are consistent with the previous results and that for any single composition the rates increase as a function of temperature. The inter-relationship between the dissolution constant (b in Eq. 4) and temperature is also shown, together with data from Shaw (2004a) on an Arrhenius plot in Fig. 4. Although the data are sparse, the activation energy for dissolution in CAS 1 and CMAS 3 can be approximated. For CAS1 the calculated activation energy is 290 kJ mol^{-1}, whereas for CMAS 3 the activation energy is similar to that quoted in Shaw (2004a), i.e. 90–110 kJ mol^{-1}. The high activation energy for slower dissolution in CAS 1 is more in line with previous estimates of activation energy for quartz dissolution in basalt of similar viscosity e.g. Donaldson (1985, 1986).

Figure 5 shows the effects of silica activity and viscosity on the dissolution constant for quartz in this study and in the earlier studies of Liang (1999) and Shaw (2004a). Figure 5a shows that for melts with viscosity lower than 1.5 Pa s, the effect of viscosity on dissolution rates is very marked (Fig. 5a): a change of viscosity of $\sim$ 1 Pa s leads to a factor of four decrease in the dissolution rate. However, for melts with viscosity greater than 1.5 Pa s even large changes in viscosity have only a minor effect on the dissolution rates. The effect of silica activity is also distinct (Fig. 5b), for all the data shown, there is a distinct decrease in the dissolution rate as the silica activity of the melt increases. For melts with the same silica activity, there are small differences in dissolution rate that are a function of the viscosity of the melt and run temperature.

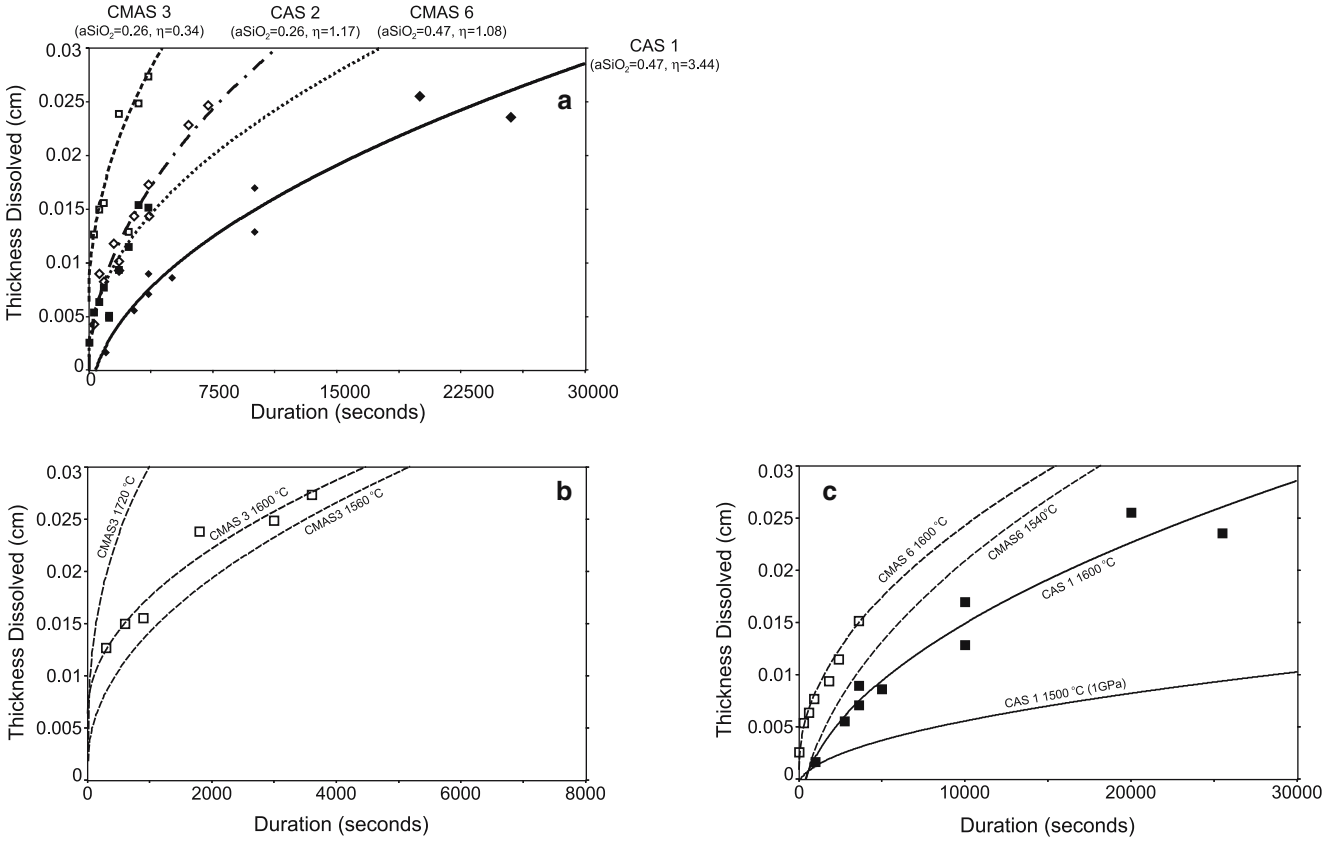

Fig. 3 **a** Data points and curves fitted by least squares regression of Eq. 4 for dissolution of quartz in melts CAS 1, CAS 2, CMAS 3, CMAS 6 at 1,600°C and 1.5 GPa. Note that dissolution thickness was calculated by mass balance using Eq. 1. **b** Comparison of data for quartz dissolution in melt CMAS 3 at 1,600°C with the dissolution amounts in CMAS 3 1,720 and 1,560°C determined by Shaw (2004a). **c** Comparison of data from this study for melts CAS 1 (*filled squares*) and CMAS 6 (*open squares*) with dissolution amounts in CMAS 6 and CAS 1 determined by Shaw (2004a) and Liang (1999), respectively

Table 4 Curve fits (Eq. 4) to the dissolution data at 1,600°C and 1.5 GPa

Solvent	Curve fit	r^2	Intercept error[a]	Slope error[a]
CAS 1	$u = -0.003754 + 0.000187\ t^{0.5}$	0.95	$\pm\ 8.76 \times 10^{3}$	$\pm\ 6.00 \times 10^{6}$
CMAS 6	$u = 0.001224 + 0.000217\ t^{0.5}$	0.96	$\pm\ 7.03 \times 10^{4}$	$\pm\ 4.10 \times 10^{7}$
CAS 2	$u = -0.000473 + 0.000287\ t^{0.5}$	0.94	$\pm\ 1.04 \times 10^{3}$	$\pm\ 4.43 \times 10^{6}$
CMAS 3	$u = 0.006415 + 0.000354\ t^{0.5}$	0.95	$\pm\ 1.68 \times 10^{3}$	$\pm\ 3.86 \times 10^{6}$

Dissolution amount (u) is given in cm s^{-1}
[a]1 sigma error to fitted curves

Melt compositions

Equilibrium experiments

Each of the melt compositions used in the dissolution experiments was equilibrated with finely ground quartz in order to determine the position of the quartz saturation surface and the solubility of SiO_2 (in mole %) in each melt at 1,600°C and 1.5 GPa. The compositions determined from experiments of 6 and 12 h duration are identical within analytical error indicating that equilibrium was attained. The quartz saturation surfaces are shown in Fig. 6 and compositions are given in Table 5. The solubility of quartz is considerably higher in CMAS melts compared to the CAS melts with the same silica activity; the difference in solubility is ~ 5 to 8 mol%. These data indicate that silica activity is not the only control on the solubility of quartz. A plot of quartz solubility against the initial NBO/T of the solvent melt (Fig. 7) for all the available data in the CMAS and CAS system shows that, with the exception of melt 4 of Shaw (2004a), quartz solubility is directly correlated with temperature and the solvent NBO/T and to a lesser extent with temperature.

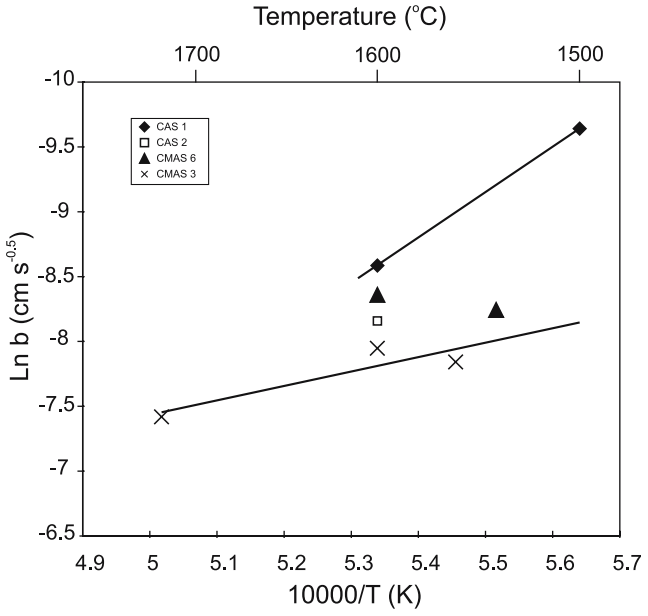

Fig. 4 Arrhenius plot of the available dissolution rate data for the solvent melts in this study together with data from Shaw (2004a)

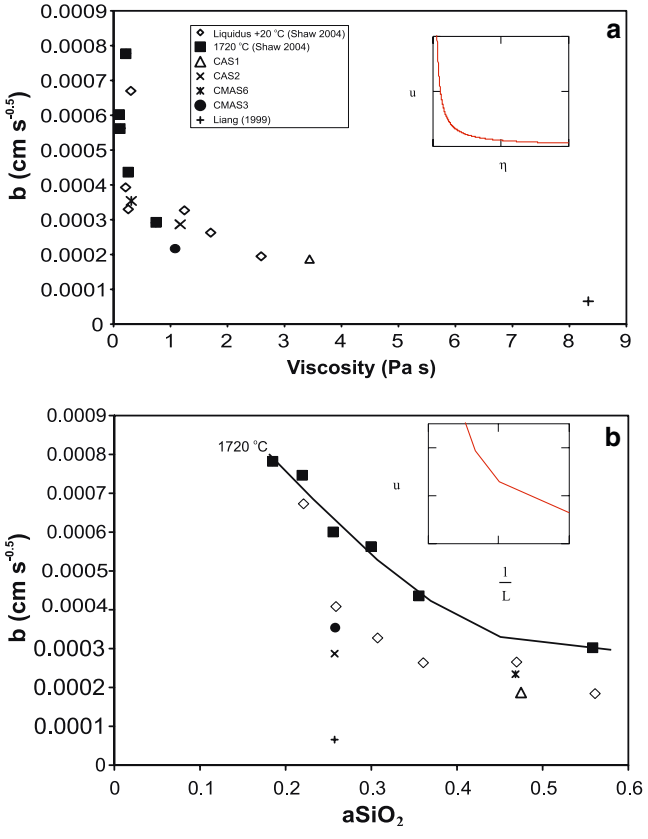

Fig. 5 Inter-relationship between **a** viscosity and the dissolution constant (parameter b in Eq. 4) and **b** silica activity and dissolution constant showing that the dissolution constant is a function of both factors. Inset graphs are calculated from Eq. 5

Dissolution experiments

Detailed compositional traverses were made perpendicular to the quartz– glass interface on all of the dissolution experiments. These data were used to: determine the amount of dissolution via mass balance calculations (see above); determine whether the far field region of the melt was contaminated during the experiment; determine the composition of the interface melts; and to obtain information on the mechanism of dissolution.

The composition of the melts in the far field region of each experiment is given in Table 6. The two longest duration CAS 1 experiments and the 60-min experiment with the CMAS 3 melt show a marked decrease in the CaO content of the melt and a small increase in the silica content relative to the starting material. These features suggest that the dissolution couple was not semi-infinite with respect to experiment duration for these three runs. They are therefore excluded from further discussion because, as Acosta-Vigil et al. (2002) and Liang (2003) pointed out interface melt compositions will vary as a function of time in systems where the dissolution couple is not semi-infinite until equilibrium between bulk liquid and mineral is achieved. Interface melt compositions for all of the experiments are given in Table 7 and are plotted in Fig. 6. Both of the CAS compositions reach interface equilibrium rapidly, i.e. the interface melts lie on the saturation surface and do not vary in composition with time. There is no significant activation time for interface saturation in the CAS 2 experiments and for CAS 1 interface saturation is reached between 2,730 and 3,600 s (45 min to 1 h). Interface compositions of melts in short duration (300–600 s) CMAS 6 experiments appear to fall on the saturation surface in Fig. 6e; however, there is a marked departure from this surface at 900 s and the interface melts in the longer experiments do not reach the saturation surface even after 1 h. However, the interface melt has an approximately constant composition after $\sim$ 1,800 s suggesting that equilibrium may have been established. Melt CMAS 3 does not approach equilibrium, even in the longest uncontaminated experiment (50 min) and all interface compositions lie far from the quartz saturation surface (Fig. 6).

Detailed electron microprobe traverses though selected samples are shown in Figs. 8 and 9. In these, compositions are plotted against distance normalized to the square root of time so that in cases where diffusion controls the dissolution process, the traverses should overlap. Four traverses in dissolution couples using melt CAS 1 (Fig. 8a) show that there is good overlap for experiments of 3,600 and 5,000 s, supporting the assertion above that local equilibrium was reached at some time between 2,730 and 3,600 s. All of the traverses in CAS 2 dissolution couples overlap (Fig. 8b), also supporting the assertion that local equilibrium was attained within 5 min or less for this composition. Traverses in the CMAS 6 dissolution couples show overlap (Fig. 9a) in experiments of 1,800 and 2,400 s indicating attainment of equilibrium, even though the compositions do not appear to lie on the

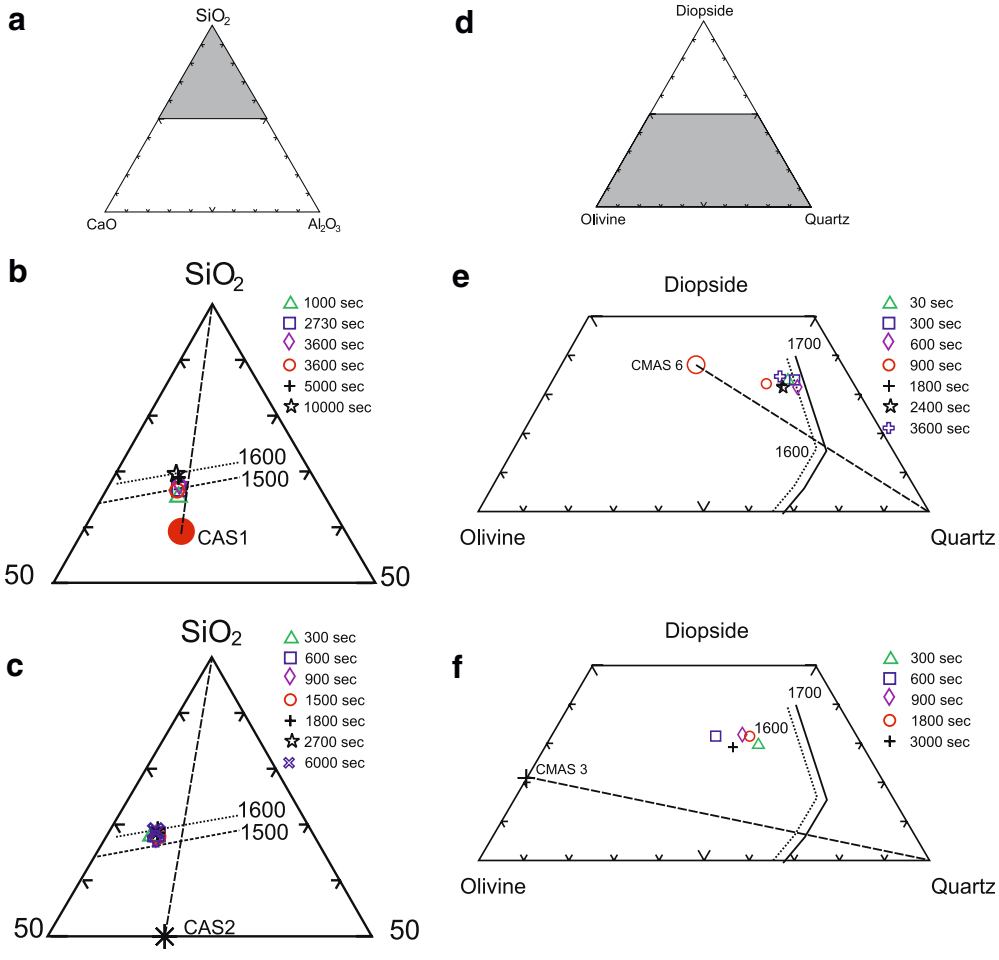

Fig. 6 Interface melt compositions for each experiment showing the quartz saturation surfaces as determined by a combination of data from Liang (1999), Shaw (2004a) and this study. *Shaded areas* in the SiO_2–CaO–Al_2O_3 and diopside–olivine–quartz ternaries indicate the regions shown in the plots. The diopside–olivine–quartz ternary is projected from plagioclase

liquidus line. However, given that the liquidus surface is interpolated from higher temperature experiments, there is the possibility of error in the position of the line.

None of the traverses in the CMAS 3 dissolution couples overlap (Fig. 9b), indicating that interface equilibrium was not attained in these experiments.

Ternary variation diagrams show well-defined trends for all oxides (Fig. 10). However, these trends are not simple binary mixing trends as shown by the deviation from the mixing lines. This indicates strong diffusive coupling along the direction of SiO_2 diffusion in compositional space.

Table 5 Composition of quartz saturated melts

Solvent	SiO_2	Al_2O_3	MgO	CaO	Total	NBO/T[a]	Solubility mol%
CAS1	70.13	11.81		18.73	100.67	0.312	26.7
CMAS 6	70.36	10.25	10.20	9.24	100.05	0.463	34.3
CAS2	69.49	11.18		19.75	100.42	0.353	40.0
CMAS 3	69.72	9.82	13.08	6.88	99.50	0.519	45.2

[a]Calculated using Mysen et al. (1984)

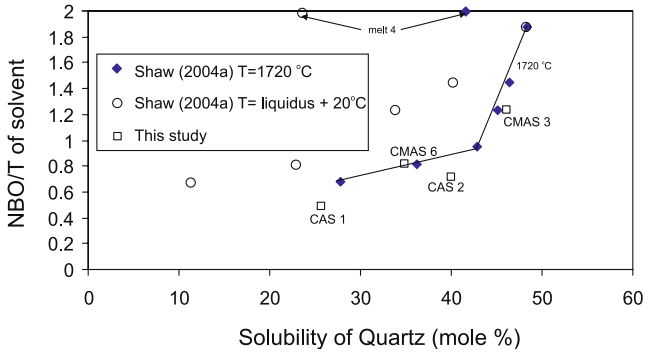

Fig. 7 Relationship of the solubility of quartz to the structure of the solvent melt as determined by NBO/T. Note that melt 4 of Shaw (2004a) does not lie on the trend. The line shows an approximate fit of the 1,720°C data

Discussion

Dissolution rates

As was shown by Shaw (2004a), dissolution rates increase with decreasing silica activity. However, for a fixed silica activity there can be significant differences in

Table 6 Far field melt compositions

Sample	Duration	Solvent	SiO_2	Al_2O_3	MgO	CaO	Total
Mo13	1,000	CAS 1	60.72	14.91	0.00	25.71	101.34
Mo10	2,730	CAS 1	60.72	15.24	0.00	24.99	100.95
Mo8	3,600	CAS 1	59.65	15.20	0.00	25.33	100.18
Mo50	3,600	CAS 1	59.47	15.01	0.00	25.25	99.73
Mo24	5,000	CAS 1	60.45	14.81	0.00	25.87	101.13
Mo25	10,000	CAS 1	60.91	14.88	0.00	26.03	101.82
Mo15	*20,000*	*CAS 1*	*60.60*	*15.37*	*0.00*	*24.12*	*100.09*
Mo 11	*25,500*	*CAS 1*	*60.47*	*15.18*	*0.00*	*24.29*	*99.94*
Mo18	*300*	*CAS 2*	*50.85*	*16.62*	*0.00*	*33.08*	*100.55*
Mo21	600	CAS 2	50.76	16.99	0.00	32.68	100.43
Mo17	900	CAS 2	50.61	17.51	0.00	32.94	101.06
Mo19	1,500	CAS 2	50.54	16.92	0.00	32.90	100.36
Mo22	1,800	CAS 2	50.59	17.55	0.00	32.13	100.27
Mo27	1,800	CAS 2	51.64	17.05	0.00	33.20	101.89
Mo23	2,700	CAS 2	50.69	17.70	0.00	32.06	100.45
Mo20	3,600	CAS 2	50.68	17.25	0.00	32.31	100.24
Mo51	3,630	CAS 2	49.29	17.10	0.00	32.89	99.28
Mo28	6,000	CAS 2	50.68	16.71	0.00	33.46	100.85
Mo16	7,200	CAS 2	50.19	17.15	0.00	32.37	99.71
Mo36	30	CMAS 6	55.26	15.18	15.25	14.41	100.10
Mo35	300	CMAS 6	54.67	15.34	15.45	14.79	100.25
Mo34	600	CMAS 6	54.74	15.20	15.35	14.67	99.96
Mo49	900	CMAS 6	54.25	15.75	15.55	14.61	100.16
Mo32	1,800	CMAS 6	54.10	16.00	15.76	14.18	100.04
Mo31	2,400	CMAS 6	53.63	15.82	15.88	13.99	99.32
Mo37	3,600	CMAS 6	55.02	15.14	15.52	14.48	100.16
Mo44	300	CMAS 3	44.37	17.38	24.96	12.82	99.53
Mo52	600	CMAS 3	44.77	17.30	24.75	12.97	99.79
Mo43	900	CMAS 3	44.18	17.43	24.63	12.91	99.15
Mo42	1,800	CMAS 3	44.78	17.58	24.31	12.41	99.08
Mo45	3,000	CMAS 3	45.06	17.12	24.78	12.73	99.69
Mo39	*3,600*	*CMAS 3*	*47.02*	*17.17*	*24.07*	*12.22*	*100.48*

Samples in italics do not show semi-infinite behaviour

Table 7 Interface melt compositions

Sample	Duration	Solvent	SiO_2	Al_2O_3	MgO	CaO	Total
Mo13	1,000	CAS 1	65.93	12.18	0.00	22.73	100.84
Mo10	2,730	CAS 1	67.12	11.53	0.00	21.82	100.47
Mo8	3,600	CAS 1	68.28	11.08	0.00	21.31	100.67
Mo50	3,600	CAS 1	67.13	11.39	0.00	22.33	100.85
Mo24	5,000	CAS 1	68.62	10.30	0.00	20.69	99.61
Mo25	10,000	CAS 1	70.22	9.77	0.00	21.00	100.99
Mo15	*20,000*	*CAS 1*	*72.60*	*8.91*	*0.00*	*18.46*	*99.97*
Mo 11	*25,500*	*CAS 1*	*71.17*	*9.31*	*0.00*	*19.26*	*99.74*
Mo18	300	CAS 2	65.08	8.07	0.00	26.80	99.95
Mo21	600	CAS 2	65.68	8.92	0.00	25.84	100.44
Mo17	900	CAS 2	64.67	8.71	0.00	26.10	99.48
Mo22	1,800	CAS 2	64.83	9.13	0.00	25.79	99.75
Mo27	1,800	CAS 2	66.40	8.38	0.00	25.22	100.00
Mo23	2,700	CAS 2	65.65	8.76	0.00	25.66	100.07
Mo20	3,600	CAS 2	66.85	8.86	0.00	25.28	100.99
Mo51	3,630	CAS 2	64.56	9.00	0.00	26.40	99.96
Mo28	6,000	CAS 2	66.14	8.28	0.00	25.81	100.23
Mo16	7,200	CAS 2	64.33	8.72	0.00	26.20	99.25
Mo36	30	CMAS 6	67.04	9.59	11.81	12.42	100.86
Mo35	300	CMAS 6	68.64	8.81	11.52	12.28	101.25
Mo34	600	CMAS 6	68.82	8.97	11.30	11.92	101.01
Mo49	900	CMAS 6	62.89	11.43	12.84	12.65	99.81
Mo32	1,800	CMAS 6	65.02	9.81	12.11	12.08	99.02
Mo31	2,400	CMAS 6	65.19	9.71	12.05	11.89	98.84
Mo37	3,600	CMAS 1	65.14	9.77	12.20	12.54	99.65
Mo44	300	CMAS 3	66.52	6.76	16.53	10.55	100.36
Mo52	600	CMAS 3	60.13	8.55	19.23	11.42	99.33
Mo43	900	CMAS 3	63.70	7.19	17.51	11.17	99.57
Mo42	1,800	CMAS 3	63.45	6.62	16.70	10.74	97.51
Mo45	3,000	CMAS 3	62.33	8.66	17.92	10.95	99.86
Mo39	*3,600*	*CMAS 3*	*62.03*	*7.36*	*18.36*	*11.41*	*99.16*

Samples in italics do not show semi-infinite behaviour

dissolution rate that can be correlated with changes in viscosity (Fig. 3a). A closer examination of all the available data suggests that at very low viscosities dissolution rates are strongly affected by small changes in viscosity. However, for viscosities between 2 and 8 Pa s, even fairly large changes in viscosity have little effect on dissolution rate (Fig. 5a). An examination of the effect of silica activity on dissolution rate shows that there is an approximately linear decrease in dissolution rate with increasing $aSiO_2$ (Fig. 5b). Meiling and Uhlmann (1967) developed an expression that relates the rate of movement of an interface to the viscosity and latent heat of dissolution / crystallization. This equation is given below

$$u = \left(\frac{k \cdot T \cdot f}{3 \cdot \pi \cdot a_o^2 \cdot \eta}\right) \times \left[1 - \exp\left(\frac{-L \cdot \Delta T}{R \cdot T \cdot T_e}\right)\right] \quad (5)$$

Where u is the growth/dissolution rate in cm s^{-1}, T is the temperature at which observations are made, f is the fraction of sites available for the detachment of atoms, k is Boltzmann's constant, a_o is the molecular diameter, η is the viscosity of the melt, L is the latent heat of dissolution, T_e is the liquidus temperature of the melt and ΔT is the degree of superheating. A plot of dissolution rate as a function of viscosity (Fig. 5a, inset) shows a very similar pattern to that observed. Similarly, if the reciprocal of the latent heat of dissolution is assumed to be proportional to the silica activity, as shown in the inset to Fig. 5b, it is also possible to reproduce the trends in the silica activity versus reaction constant plot. There is, however, an apparent temperature dependence in the silica activity–dissolution constant data (Fig. 5b) that is not seen in the viscosity–dissolution constant plot.

Solubility of quartz

The equilibration experiments show that the solubility of quartz in the various solvent melts, both in this study and in that of Shaw (2004a) is dependent on the silica activity of the melt (and similar parameters such as thermodynamic affinity and optical basicity) and the viscosity (or NBO/T) of the solvent melt (Fig. 7). Similarly, there is an apparent temperature dependence between solubility and the dissolution constant (Fig. 11), although there are very few data at present to determine if solubilities could be used as a predictive tool for dissolution rates.

Why parabolic kinetics?

One of the key factors in the identification of diffusion as a major control of dissolution rates is that the amount of

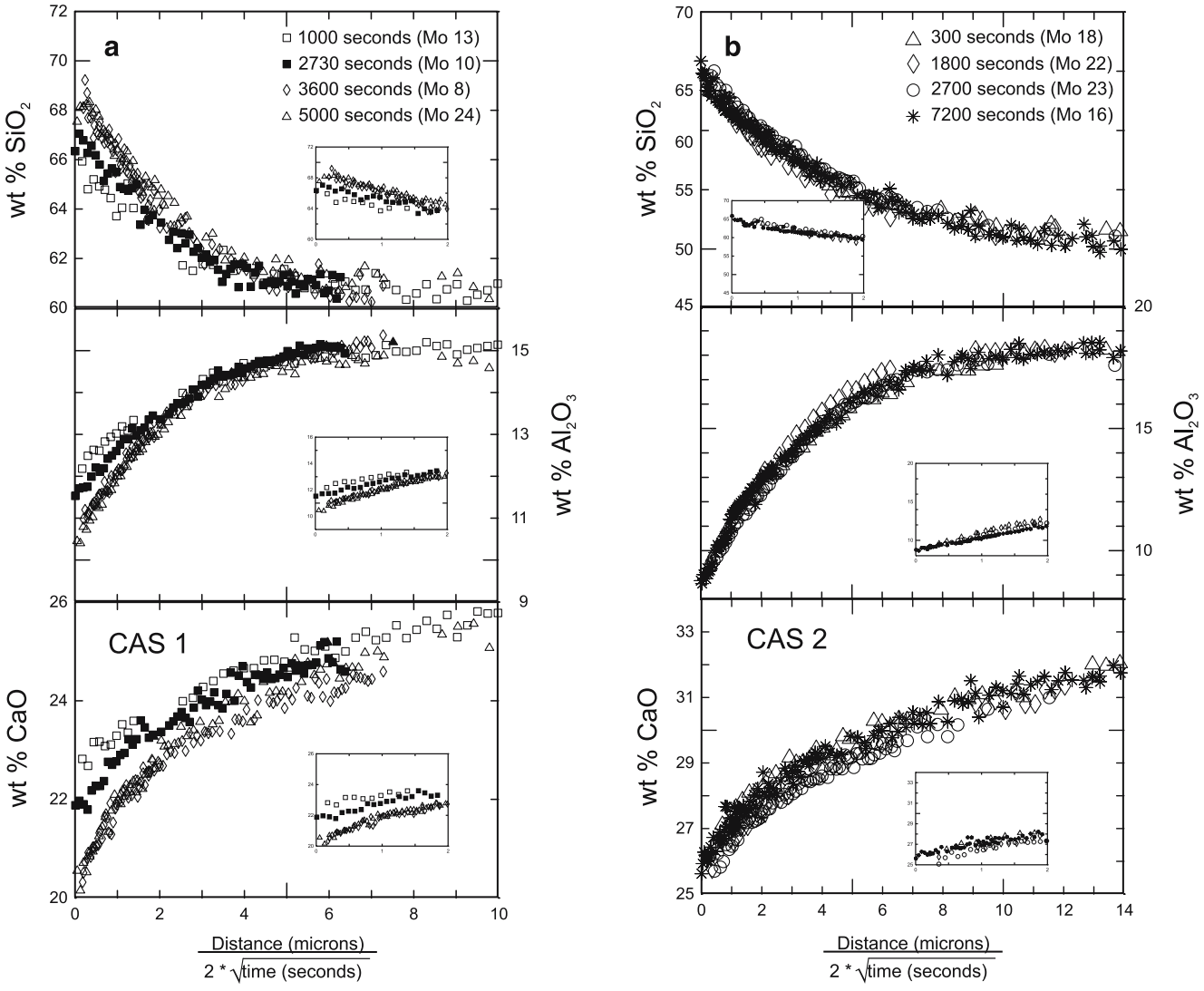

Fig. 8 Plot of oxide composition against distance normalized to the square-root of time for melts CAS1 and CAS 2. Note that in CAS 1 only profiles from Experiments Mo 8 and Mo 24 overlap indicating a significant activation time for diffusion control. Conversely all data for CAS 2 overlap showing that the activation time is less than 300 s

quartz dissolved is proportional to the square-root of time. However, even in reactions where chemical data clearly point to transient control by interface kinetics, the resulting data still give parabolic kinetics within the limits of error of the dissolution measurements. Tiller (1991) presented examples where the growth rate was proportional to $t^{0.5}$ during interface controlled crystallization. Tiller noted that a $t^{0.5}$ relation implies only that the Gibbs free energy of the reaction is constant.

Dissolution mechanisms

Although there are a number of possible rate-controlling processes during mineral dissolution reactions (see Shaw (2000) for a review), only two, interface reaction kinetics and diffusion of cations away from the reaction site, are considered to be important for silicate minerals (see also Kirkpatrick 1975). Of these, it is generally assumed that diffusion will be rate controlling in melts of geological interest, based on the modelling of Zhang et al. (1989). This assumption is supported by reports in the material science literature; however, Jackson and Mills (1997) added the caveat that this behaviour is only known in high viscosity systems.

An examination of the geological literature (e.g. Shaw 2004a) shows that in most experimental mineral dissolution studies where the rate control has been assessed, interface saturation is reached rapidly and thus diffusion controls the rate at which the mineral dissolves (e.g. Liang 1999; Watson 1982; Zhang et al. 1989). Liang (1999) and Zhang et al. (1989) have suggested that interface reaction is unlikely to control dissolution in geologically relevant melts. However, Acosta-Vigil et al. (2002), Hammouda and Pichavant (1999) and Shaw (2000, 2004a) have suggested that it can occur although it

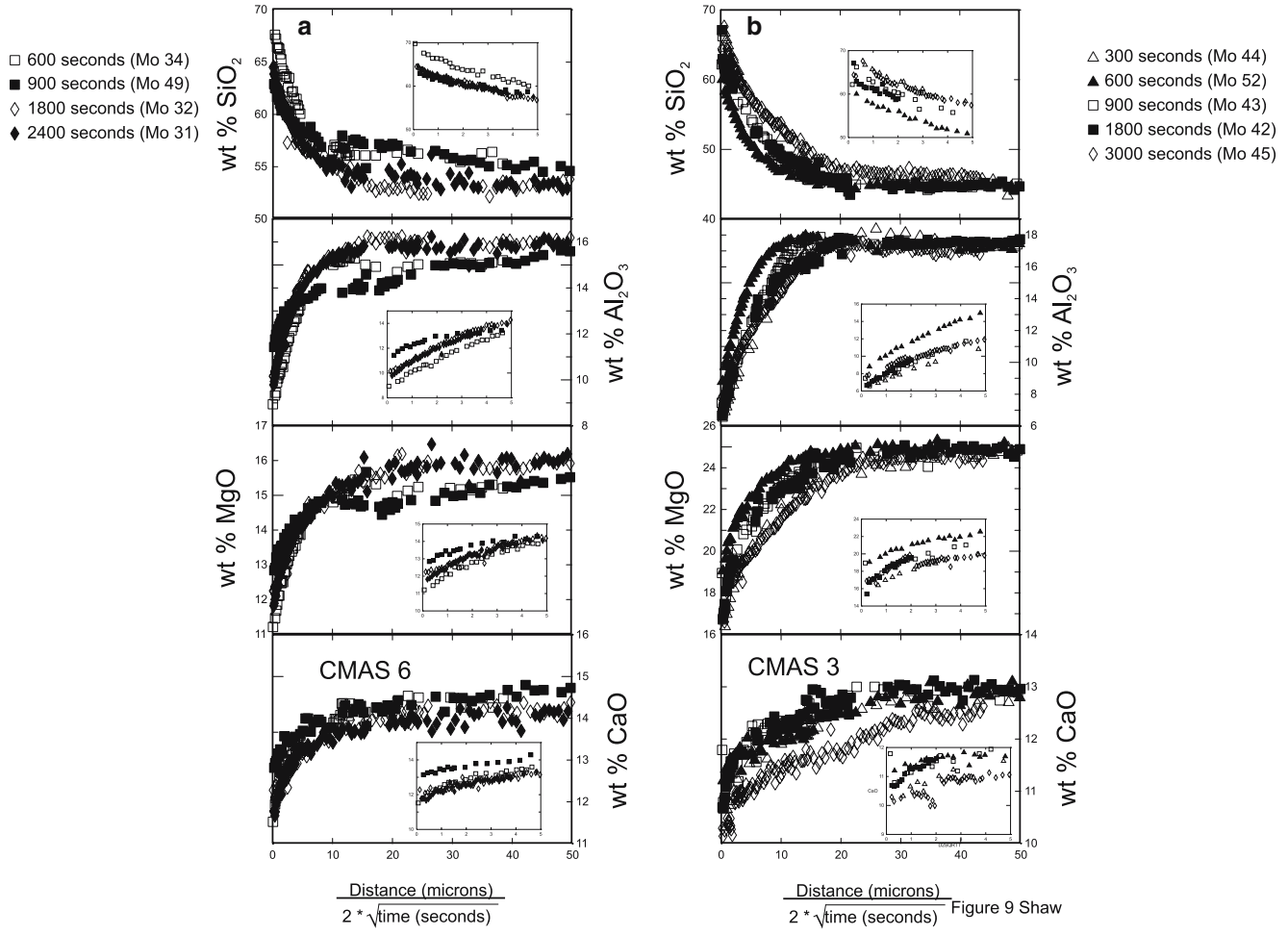

Fig. 9 Plot of oxide composition against distance normalized to the square-root of time for melts CMAS 6 and CMAS 3. Note the overlap in the 1,800 and 2,400 s profiles for CMAS 6 and the lack of overlap in all profiles for melt CMAS 3

is a transient control that may last for minutes to hours before the reaction is eventually limited by diffusion.

In the following discussion, I refer to reactions being controlled by diffusion if there is a clear evidence of interface saturation within $\sim 10^2$ s, which represents an order of magnitude more than the critical time implied by Zhang et al. (1989) for most dissolving systems. A reaction is considered interface controlled, albeit transiently, if more than 10^3 s are required for interface saturation to be achieved. Using these criteria, quartz dissolution in CAS 2 is diffusion controlled, whereas dissolution in both CMAS melts and in CAS 1 is controlled by interface kinetics (Figs. 6, 8, 9). The interface control of dissolution in CAS 1 is at odds with the interpretation of rapid attainment of interface equilibrium in the same melt at 1,500°C (Liang 1999). Zhang et al. (1989) and Shaw (2004a) have noted that the rate-controlling step in dissolution is a function of the interplay between diffusion and interface reaction kinetics. The observation of a significant period of interface control for CAS 1 at 1,600°C and its absence at 1,500°C suggests that for this composition the increase in diffusion rate with increasing temperature (~ a factor of 3, Liang and Davis 2002) outpaced the interface reaction rate leading to a switch in the dissolution regime (see Figure 14 of Shaw 2004a).

What controls the dissolution mechanism?

Shaw (2004a) suggested that while the degree of silica undersaturation of a solvent melt is important, melt viscosity also plays a role in determining both the rate and mechanism of quartz dissolution in simple synthetic silicate melts. The new data presented here, together with the published data of Liang (1999) and Shaw (2004a), permit a more detailed evaluation of this hypothesis.

It is worth noting that although many of the melts that show significant activation times are of low viscosity and would therefore be expected to have rapid diffusion, there are at least two very viscous melts in which diffusion is slow but there is a very long activation time for attainment of interface saturation. Although

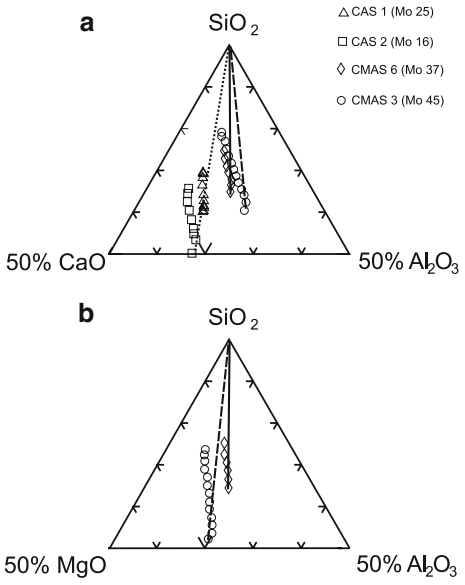

Fig. 10 Ternary plots of melt composition from four selected experiments showing that the boundary layer melts do not lie on simple binary mixing lines suggesting that there is diffusive coupling between the cations during quartz dissolution. CMAS data are projected from MgO in **a** and from CaO in **b**

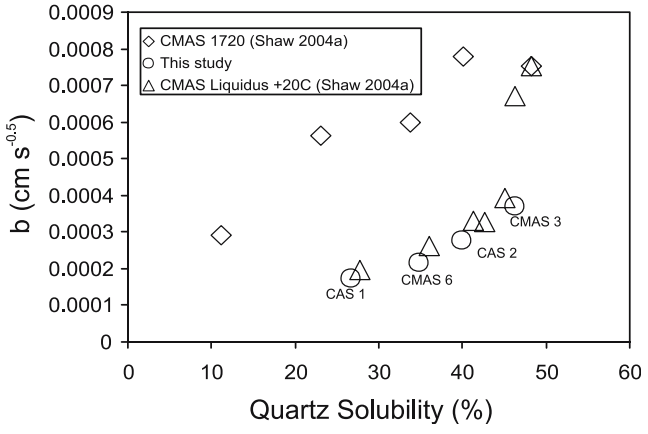

Fig. 11 Relationship between quartz solubility and the dissolution constant in the experiments reported in this study and in the work of Shaw (2004a). Note the linear trend for the 1,720 and 1,600°C data indicating that both parameters are also a function of temperature

data on intermediate compositions are not yet available, it seems possible that there are three domains of viscosity–activity relations (Fig. 12). In domain I, the time required for interface saturation is greater than 10^5 s. This type of behaviour appears to be limited to very high viscosity melts. Domain II also shows interface control; however, it is limited to durations between 10^3 and 10^5 s. The melts that show this type of behaviour are generally of low viscosity. Domain III melts establish interface saturation in less than 10^3 s and tend to be of intermediate viscosity; however, the experimental database is still too small to define this relationship with any degree of certainty.

The occurrence of three domains of dissolution behaviour suggests that the interface reaction rate may be non-linear such that there is a significant period required for interface saturation to be achieved in both low and high viscosity melts (see Fig. 12 inset).

Dissolution and melt structure

If we consider all the available data in the CAS and CMAS system (Fig. 13), it is clear that there is a temperature-dependent relationship between dissolution and the structure of the silicate melt, as defined by NBO/T, i.e. the ratio of non-bridging to tetrahedral coordinated oxygens. For NBO/T from 0.5 to 1.5 the dissolution rate of quartz increases with increasing NBO/T; however, there appears to be an inflection at NBO/T $\sim$ 1.5 after which the dissolution rate decreases with increasing NBO/T.

These data can be interpreted in two ways. First, there may be a real discontinuity in the dissolution rate as a function of melt structure, regardless of composition. Alternatively, there may be two separate trends, one for aluminous melts and another for Al-poor to Al-free melts. At present there are very few data to distinguish between these two hypotheses.

Geological applications

Infiltration of melt along grain boundaries is an important process in mantle metasomatism (e.g. Shaw et al. 2005) and in the segregation and transport of granitic melts into and out of migmatite systems (e.g. Lupulescu and Watson 1999 and references therein). Melts infiltrating during mantle metasomatism are likely to be of low viscosity and depending on their composition, they may be highly reactive (Shaw et al. 1998, 2005; Shaw 1999). In such a scenario, there are two possible consequences of interface-controlled reaction. First, if there is a continuous flow of melt, the dissolution couple may never reach interface saturation, thus the dissolution rate will be controlled by reaction kinetics for the entire period of melt flow. If estimates of reaction time are based only on diffusion rates in the melt when in fact rates were controlled by interface processes, the estimates will be too low. Second, the composition of secondary melts formed during reaction may be far from that predicted by equilibrium experiments or binary mixing calculations in part due to the interface control and because of the strong diffusive coupling that is common during dissolution reactions.

Similar scenarios of grain boundary infiltration are likely to arise in granitic systems and in fact, Acosta-Vigil et al. (2002, 2006) have documented very long periods of interface-controlled dissolution in haplogranitic systems. However, the higher viscosity of granitic

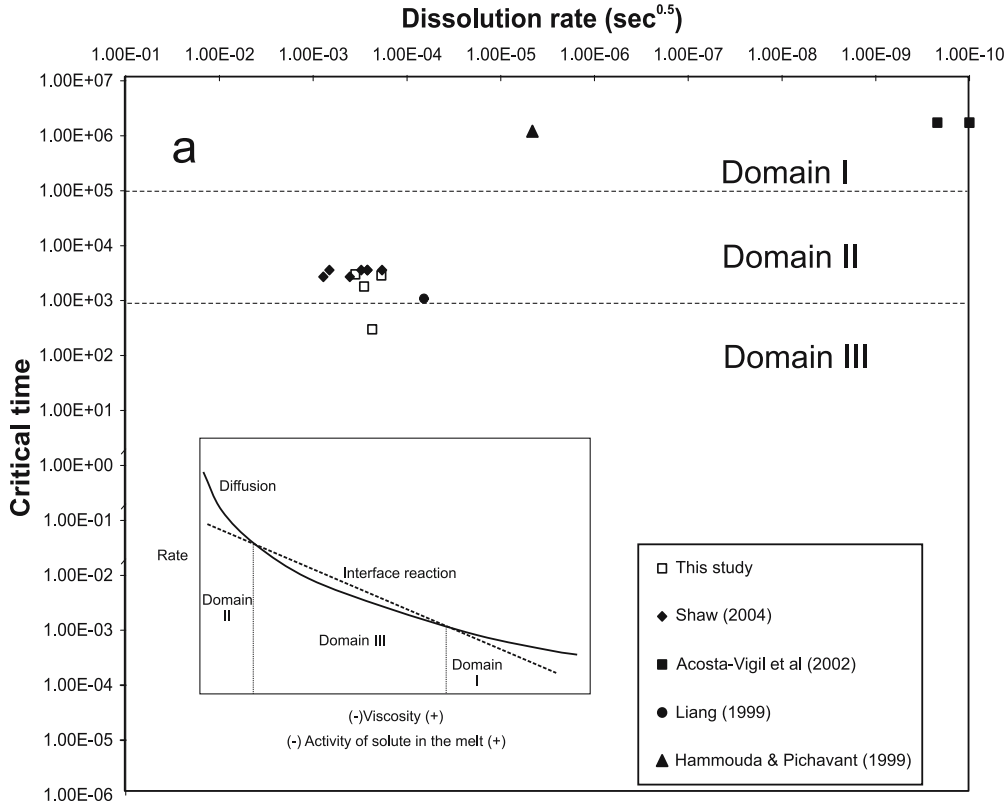

Fig. 12 Dissolution rate versus critical time plot showing that the current database of dissolution rate data can be divided into three domains. In domain I dissolution does not become diffusion controlled until > 10^5 s. Melts in domain II require between 10^3 and 10^5 s for diffusion to become rate controlling. Melts in domain III reach interface saturation in less than 10^3 s; these are the only melts that conform to the predictions of Zhang et al. (1989). The *inset* shows the relationship between diffusion and interface reaction rate and melt/solute properties required to explain the domains

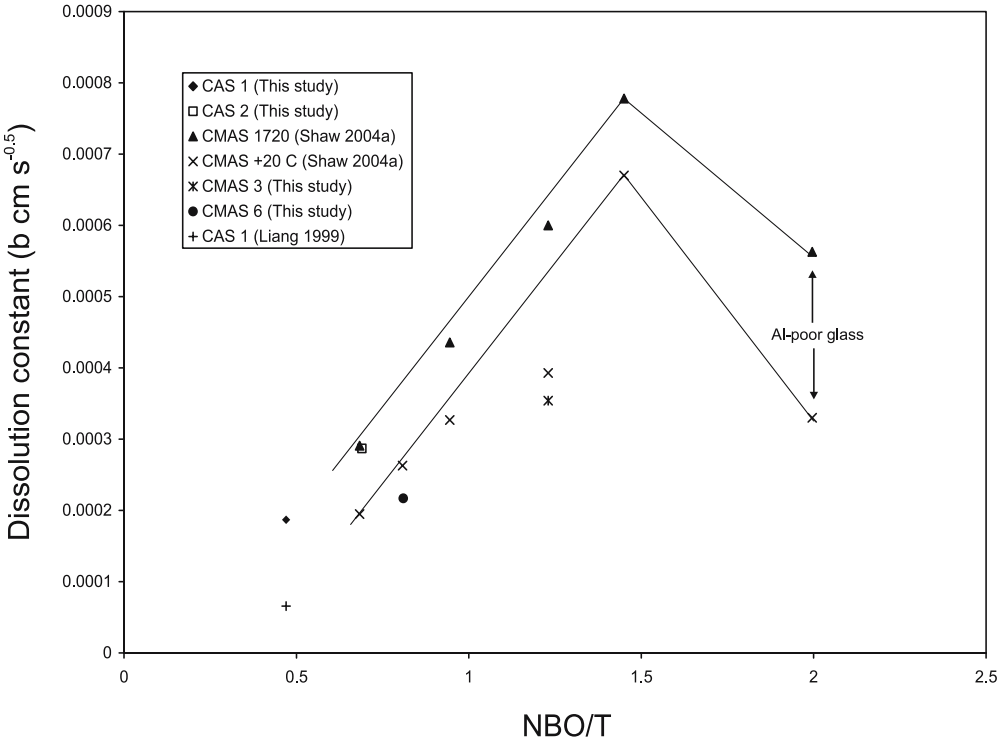

Fig. 13 NBO/T—dissolution rate plot showing an apparent inflection at NBO/T 1.5 (see text for details)

relative to basaltic melts suggests that flow rates are likely to be smaller and the effects of a transient period of interface control may have smaller effects in granitic systems.

Conclusions

1. Quartz dissolution in melts with low silica activity is faster than that in melts with higher silica activity regardless of the viscosity of the melts.
2. For melts with the same silica activity, the dissolution rate is fastest in the melt with the lowest viscosity.
3. The control on the transient period of interface control has not yet been clearly established, the simple prediction from the earlier data of Shaw (2004a) is not supported by the data from this study. Further detailed studies of other melt compositions and solute minerals will be required to solve this problem, which appears to be related not only to thermodynamic parameters but also to the structure of the melt.
4. The solubility of quartz shows a linear relationship to the dissolution constant suggesting that solubility may be a useful parameter for estimating dissolution rates.

Acknowledgements Thanks to Ancel Murphy for preparing the polished sections, Rhonda MacDonald for preparing and polishing the quartz discs and Douglas Hall for his assistance with the SEM and microprobe analyses. I am also grateful to Don Dingwell for discussions on the role of melt structure in the dissolution of quartz and for the use of the rotational viscometer at Ludwig-Maximilians Universität, München. This work was funded by a Discovery grant from the Natural Sciences and Engineering Research Council. Part of this work was carried out while the author was supported by the Alexander von Humboldt Foundation. I am very grateful to Kelly Russell and Antonio Acosta-Vigil for their thorough and constructive reviews of this work.

References

Acosta-Vigil A, London D, Dewers TA, Morgan GB (2002) Dissolution of corundum and andalusite in H_2O-saturated haplogranitic melts at 800°C and 200 MPa: constraints on diffusivities and the generation of peraluminous melts. J Petrol 43(10):1885–1908

Acosta-Vigil A, London D, Morgan GB, Dewers TA (2006) Dissolution of quartz, albite and orthoclase in H_2O-saturated haplogranitic melt at 800°C and 200 MPa: diffusive transport properties of granitic melts at crustal anatectic conditions. J Petrol 47:231–254

Apanina AT (1984) Corrosion resistance of refractories in molten borosilicate frit. Glass Ceram 41:486–487

Avramov I, Pascova R, Samouneva B, Gutzow I (1979) The mechanism of crystallisation and dissolution of $LiPO_3$ from its melt. Phys Chem Glasses 20:91–96

Barnes CG, Dumond G, Yoshinobu AS, Prestvik T (2004) Assimilation and crystal accumulation in a mid-crustal magma chamber: the Sausfjellet pluton, north-central Norway. Lithos pp 389–412

Brearley M, Scarfe CM (1986) Dissolution rates of upper mantle minerals in an alkali basalt melt at high pressure: an experimental study and implications for ultramafic xenolith survival. J Petrol 27:1157–1182

Canil D, Fedortchouk Y (1999) Garnet dissolution and the emplacement of kimberlites. Earth Planet Sci Lett 167:227–237

Chakraborty S, Dingwell DB, Rubie DC (1995) Multicomponent diffusion in ternary silicate melts in the system $K_2O - Al_2O_3 - SiO_2$: II. Mechanisms, systematics and geological applications. Geochim Cosmochim Acta 59:265–277

Cooper AR, Kingery WD (1964) Dissolution in ceramic systems: I, Molecular diffusion, natural convection, and forced convection studies of sapphire dissolution in calcium aluminum silicate. J Am Ceram Soc 47:37–43

Dingwell DB (1989) Shear viscosities of ferrosilicate liquids. Am Mineral 74(9–10):1038–1044

Donaldson CH (1985) The rates of dissolution of olivine, plagioclase, and quartz in a basalt melt. Mineral Mag 49:683–693

Donaldson CH (1986) Mineral dissolution rates in a superheated basalt melt. Mater Sci Forum 7:267–274

Donaldson CH (1990) Forsterite dissolution in superheated basaltic, andesitic and rhyolitic melts. Mineral Mag 54:67–74

Edwards BR, Russell JK (1996) A review and analysis of silicate mineral dissolution experiments in natural silicate melts. Chem Geol 130:233–245

Edwards BR, Russell JK (1998) Time-scales of magmatic processes: new insights from dynamic models for magmatic assimilation. Geology 26:1103–1106

Ghiorso MS, Sack RO (1995) Chemical mass transfer in magmatic processes. IV. A revised and internally consistent thermodynamic model for the interpolation and extrapolation of liquid–solid equilibria in magmatic systems at elevated temperatures and pressures. Contrib Mineral Petrol 119:197–212

Gurenko AA, Chaussidon M, Schmincke H-U (2001) Magma ascent and contamination beneath one intraplate volcano: evidence from S and O isotopes in glass inclusions and their host clinopyroxenes from Miocene basaltic hyaloclastites southwest of Gran Canaria (Canary Islands). Geochim Cosmochim Acta 65:4359–4374

Hammouda T, Pichavant M (1999) Kinetics of melting of fluorphlogopite–quartz pairs. Eur J Mineral 11: 637–653

Jackson MJ, Mills B (1997) Dissolution of quartz in vitrified ceramic materials. J Mater Sci 32:5295–5304

Kalyanram MR, Bell HB (1960) The activity of calcium oxide in slags in the systems $CaO-MgO-SiO_2$, $CaO-Al_2O_3-SiO_2$ and $CaO-MgO-Al_2O_3-SiO_2$ at 1,500°C. J Iron Steel Inst 195:58–64

Kelemen PB, Dick HJB, Quick JE (1992) Formation of harzburgite by pervasive melt/rock reaction in the upper mantle. Nature 358:635–641

Kerr RC (1995) Convective crystal dissolution. Contrib Mineral Petrol 121:237–246

Kirkpatrick RJ (1975) Crystal growth from the melt: a review. Am Mineral 60:798–814

Lange R, Carmichael ISE (1987) Densities of $Na_2O-K_2O-CaO-MgO-$ $FeO-Fe_2O_3$ $-Al_2O_3-TiO_2$ SiO_2 liquids; new measurements and derived partial molar properties. Geochim Cosmochim Acta 51:2931–2946

Liang Y (1999) Diffusive dissolution in ternary systems: analysis with applications to quartz and quartzite dissolution in molten silicates. Geochim Cosmochim Acta 63:3983–3995

Liang Y (2003) Kinetics of crystal-melt reaction in partially molten silicates. Geochem Geophys Geosyst 4:1–27

LiangY, Davis AM (2002) Energetics of multicomponent diffusion in molten $CaO-Al_2O_3-SiO_2$. Geochim Cosmochim Acta 66:635–646

Lupulescu A, Watson E (1999) Low melt fraction connectively of granitic and tonaltic melts in a mafic crustal rock at 800°C and 1 GPa. Contrib Mineral Petrol 134:202–216

Maury RC, Didier J (1991) Xenoliths and the role of assimilation. In: Didier J, Barbarin B (eds) Enclaves and granite petrology. Developments in petrology. Elsevier, Amsterdam, pp 529–542

Meiling GS, Uhlmann DR (1967) Crystallisation and melting kinetics of sodium disilicate. Phys Chem Glasses 8:62–68

Mysen BO, Virgo D, Seifert FA (1984) Redox equilibria of iron in alkaline earth silicate melts: relationships between melt structure, oxygen fugacity, temperature and properties of iron-bearing silicate liquids. Am Mineral 69:834–847

Shaw HR (1972) Viscosities of magmatic silicate liquids: an empirical method of prediction. Am J Sci 272:870–893

Shaw CSJ (1999) Dissolution of orthopyroxene in basanitic magma between 0.4 and 2 GPa: further implications for the origin of Si-rich alkaline glass inclusions in mantle xenoliths. Contrib Mineral Petrol 135:114–132

Shaw CSJ (2000) The effect of experiment geometry on the mechanism and rate of dissolution of quartz in basanite at 0.5 GPa and 1,350°C. Contrib Mineral Petrol 139:509–525

Shaw CSJ (2004a) Mechanisms and rates of quartz dissolution in melts in the CMAS ($CaO-MgO-Al_2O_3-SiO_2$) system. Contrib Mineral Petrol 148:180–200

Shaw CSJ (2004b) The temporal evolution of three magmatic systems in the West Eifel volcanic field, Germany. J Volcanol Geotherm Res 131:213–240

Shaw CSJ, Thibault Y, Edgar AD, Lloyd FE (1998) Mechanisms of orthopyroxene dissolution in silica-undersaturated melts at 1 atmosphere and implications for the origin of silica-rich glass in mantle xenoliths. Contrib Mineral Petrol 132: 354–370

Shaw CSJ, Eyzaguirre J, Fryer BJ, Gagnon J (2005) Regional variations in the mineralogy of metasomatic assemblages in mantle xenoliths from the West Eifel volcanic field, Germany. J Petrol 46:945–972

Tiller WA (1991) The science of crystallization: microscopic interfacial phenomena. Cambridge University Press, New York pp 391

Toplis MJ, Dingwell DB (2004) Shear viscosities of $CaO-Al_2O_3-SiO_2$ and $MgO-Al_2O_3-SiO_2$ liquids: implications for the structural role of aluminum and the degree of polymerisation of synthetic and natural aluminosilicate melts. Geochim Cosmochim Acta 68:5169–5188

Watson EB (1982) Basalt contamination by continental crust: some experiments and models. Contrib Mineral Petrol 80:73–87

Watson EB (1996) Dissolution, growth and survival of zircons during crustal fusion: kinetic principles, geologic models and implications for isotopic inheritance. Trans R Soc Edin Earth Sci 87:43–56

Zhang Y, Walker D, Lesher CE (1989) Diffusive crystal dissolution. Contrib Mineral Petrol 102:492–513